



Cite this: DOI: 10.1039/c9cp02900a

fs-ps Exciton dynamics in a stretched tetraphenylsquaraine polymer†

 Maximilian H. Schreck, Lena Breitschwerdt, Henning Marciniak, Marco Holzapfel, David Schmidt, Frank Würthner  and Christoph Lambert *

A tetraphenylsquaraine was synthesized whose structure was elucidated by single crystal X-ray structure analysis. Unlike all known indolenine squaraines, the tetraphenylsquaraine shows an unusual nonplanar structure with the four phenyl groups pointing away from the squaric acid core in order to avoid steric congestion. This tetraphenylsquaraine was polymerized by a Yamamoto coupling to form a conjugated polymer with $X_n = 38$. The absorption spectra of this polymer are red-shifted compared to that of the monomer and show a J-type absorption band due to exciton coupling. Transient absorption spectra with fs-time resolution display a strong ground state bleaching signal with a peak on the red side rising concurrently with the decay of a peak on the blue side of an isosbestic point at 12000 cm^{-1} . This behavior is caused by energy transfer between two slightly different sections of the polymer with time constants of 0.3 and 2.6 ps. According to semiempirical calculations these different sections are stretched and slightly bent conformations of the polymer strand. Power dependent transient absorption measurements indicate exciton annihilation which also proves the excitons to be very mobile.

Received 22nd May 2019,
Accepted 22nd June 2019

DOI: 10.1039/c9cp02900a

rsc.li/pccp

Introduction

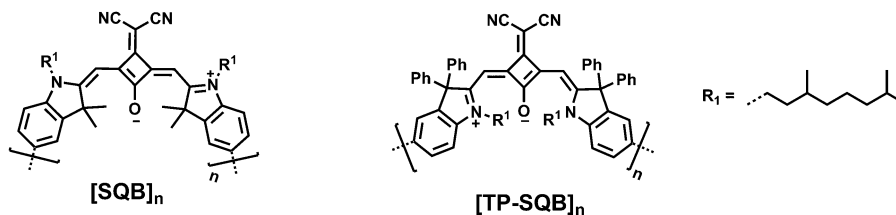
Conjugated polymers are one of the key players in organic electronics^{1–4} as they can be used as emitters in OLEDs,⁵ as light absorbing materials in organic photovoltaic (OPV) devices,^{6–8} in bioelectronics⁹ and as transport materials in organic field effect transistors (OFET).^{10,11} Here the monomeric constituents of the polymers are usually small aromatic or heteroaromatic units such as benzene, thiophene or pyrrole or even more complex heterocycles such as benzothiadiazole, either annulated, directly linked *via* single bonds, or *via* other π -bridges such as conjugated CC-double or triple bonds. In these polymers the optical and electrical properties are largely determined by the conjugative interaction of the monomers which leads to quite distinct optoelectronic properties of the polymers compared to their monomeric constituents. On the other hand, molecular conjugated materials¹² and dyes such as diketopyrrolopyrroles, merocyanines, perylenedimides, BODIPYs or squaraine dyes^{13–18} may substitute conjugated polymers in the above mentioned applications or may even be superior as for example in OFETs.^{19–23} Here, the electronic and optical properties are inherent to the chromophore unit but supramolecular arrangement and morphology also

play an important role. The latter squaraine dyes are somewhat exceptional because of their intense and narrow absorption band in the red to near infrared spectral region and their high fluorescence quantum yield.^{24,25} Unlike cationic cyanine dyes, which show similar optical properties, squaraine dyes are electrically neutral and soluble in common organic solvents. Between the two extremes, conjugated polymers on the one hand and molecular dyes on the other, oligomers or polymers formed by covalent linking of molecular dyes represent an attractive alternative with often more predictable electronic properties.^{26,27} In these covalently linked “aggregates”, the optical properties can successfully be understood by simple exciton coupling of localized transition dipole moments which yields an exciton manifold to which transitions may be allowed or forbidden, depending on the relative orientation of the transition dipole moments.²⁸ For example, linear BODIPY oligomers in which the relative orientation of the chromophores is locked by appropriate alky substituents, show distinct exchange narrowing of the J-type absorption band indicative of a strong delocalization of the exciton²⁹ while oligomers of other BODIPYs show helix formation with H-aggregate behavior.³⁰ Similar effects were observed for homo and heteropolymers of squaraine dyes.^{13,31,32} Such oligomers and polymers have also successfully been used in OPV¹³ and NIR OLEDs.³³

In general, polymerization of suitable monomeric squaraine dyes leads to polysquaraines whose optical properties not only depend on the chemical nature of the squaraine monomers but also on the mutual arrangement of the squaraine dyes within the polymer strand, that is, the polymer folding structure.³⁴

Institute of Organic Chemistry, Center for Nanosystems Chemistry, Universität Würzburg, Am Hubland, D-97074 Würzburg, Germany.
E-mail: christoph.lambert@uni-wuerzburg.de

† Electronic supplementary information (ESI) available. CCDC 1916888. For ESI and crystallographic data in CIF or other electronic format see DOI: 10.1039/c9cp02900a



Scheme 1 Polymer structure of $[\text{SQB}]_n$ and of $[\text{TP-SQB}]_n$.

This is because within the exciton coupling theory the relative orientation of localized transition dipole moments is decisive for the resulting states of the exciton manifold and their transition probability.³⁵ Recently we showed that a polymer $[\text{SQB}]_n$ (see Scheme 1) built up from a *cis*-squaraine may form stretched or helical foldamers, depending on the solvent environment.^{13,32} While the former shows typical J-type aggregate behavior, that is, an intense and red-shifted absorption band, the helices display typical H-type aggregate bands with the main absorption blue-shifted. In order to control the polymer structure, and thereby also the optical properties, we designed a new tetraphenyl-*cis*-squaraine monomer which, owing to four sterically demanding phenyl substituents, should form a stretched polymer strand $[\text{TP-SQB}]_n$ (see Scheme 1) rather than a helical foldamer, irrespective of the used solvent. The optical properties, in particular the photoinduced dynamics of this polymer are in focus of this work.

Experimental

The synthetic protocols can be found in the ESI.†

Absorption spectra were measured with a Jasco V-570 or V-670 UV/vis/NIR spectrometer in 1 mm or 10 mm quartz cuvettes and referenced against the pure solvent.

An Edinburgh Instruments FLS980 fluorescence lifetime spectrometer was used for steady state fluorescence measurements, determination of fluorescence quantum yields and fluorescence lifetime measurements. The observed fluorescence quantum yields were determined with an integration sphere and afterwards corrected for self-absorption applying the method of Bardeen *et al.*³⁶ Fluorescence lifetimes were determined by time-correlated single-photon counting (TCSPC).

Transient absorption measurements were performed using a Helios transient absorption spectrometer from Ultrafast Systems. The pump pulses were generated with a noncollinear optical parametric amplifier (NOPA), and compressed with a fused silica prism compressor to durations of under 25 fs. White light generation in 3 mm sapphire plates in the Helios spectrometer as well as in the NOPA was seeded with 900 nm pulses from a TOPAS-C (Light Conversion) to achieve pump and probe wavelengths near the fundamental wavelength of the laser source (800 nm). A Solstice amplified Ti:sapphire laser from Newport Spectra-Physics served as pulse source for the whole setup. The sample solutions in CHCl_3 were pumped through a flow cell (Starna) with 0.2 mm thick quartz windows and 0.2 mm path length during the measurements, using a micro annular gear pump (HNP Mikrosysteme). The spot size of the pump pulses on

the samples was approx. 250 μm in radius, estimated from pump energy measurements before and after a pinhole. The spot size of the probe pulses was significantly smaller with a radius of approx. 125 μm .

Results and discussion

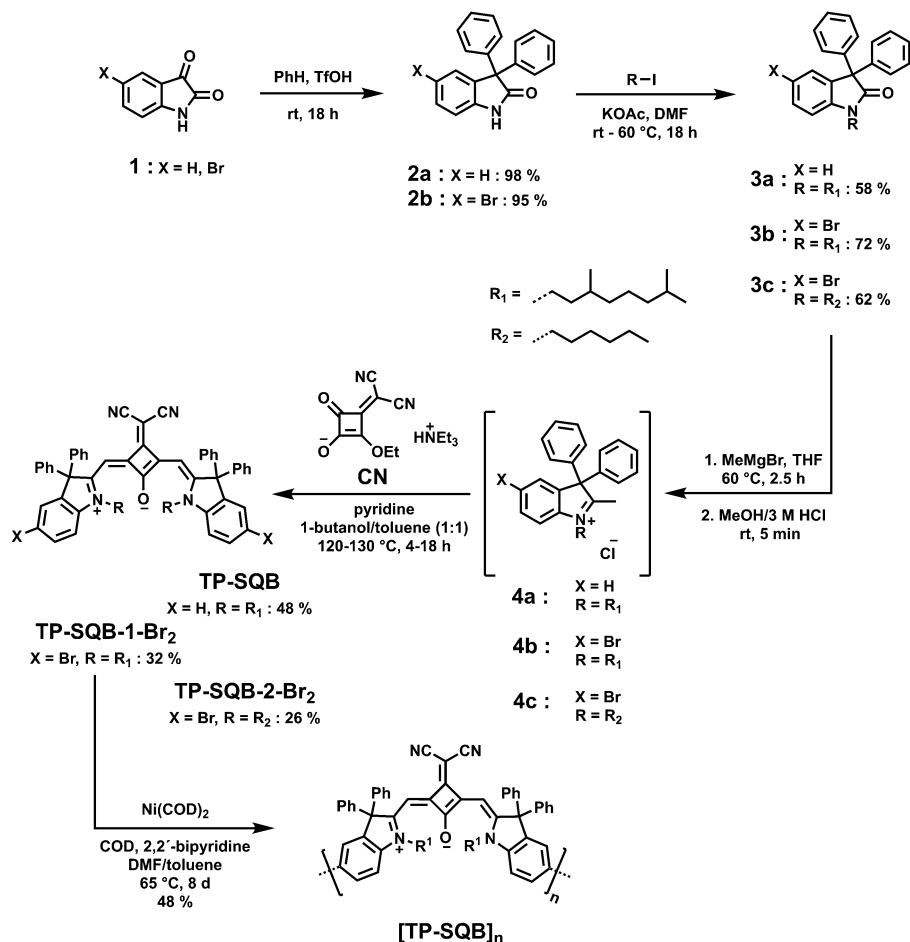
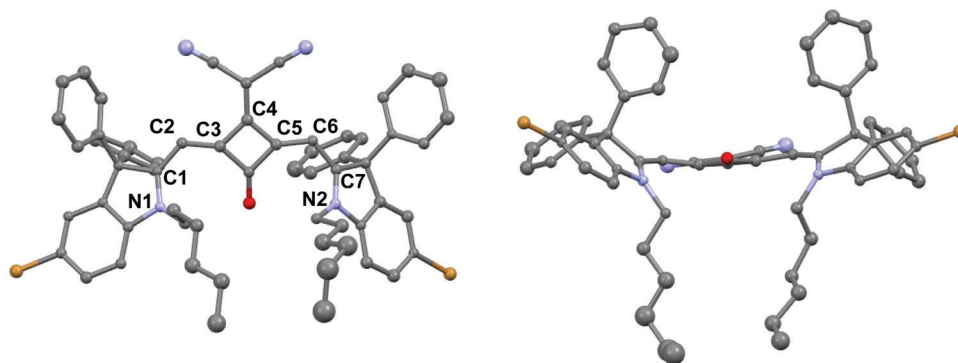
Synthesis and structure

The monomer **TP-SQB** and its bromo derivative **TP-SQB-1-Br₂** were synthesized as presented in Scheme 2. Also a bromo derivative with hexyl side chains instead of the dimethyloctyl chains was prepared.

By acidic activation of isatin **1** with TfOH an electrophilic substitution at benzene yielded the diphenyloxindoles **2a** and **2b** which were alkylated subsequently by the appropriate alkyl halide at the nitrogen to give lactams **3a–3c**. Reaction with a methyl Grignard reagent and subsequent elimination gave the iminium salts which proved to be unstable³⁷ and were therefore used without further purification. Deprotonation with a weak base (pyridine) and reaction with dicyanomethylene squaric acid ethyl ester gave the desired squaraine dyes. In this context it is worth mentioning that debromination is a severe side reaction for **4b** and **4c** which could be suppressed by applying inert gas atmosphere and short reaction times (*ca.* 4 h).

Polymerization of **TP-SQB-1-Br₂** was achieved by Yamamoto homocoupling reaction with Ni(COD), see Scheme 2. The crude polymer was purified by Soxhlet extraction with hexane, MeOH and finally acetone. The acetone extract was fractionated by preparative GPC and afforded a batch with $M_n = 36\,600$ and PDI = 2.35 with a degree of polymerization $X_n = 38$.

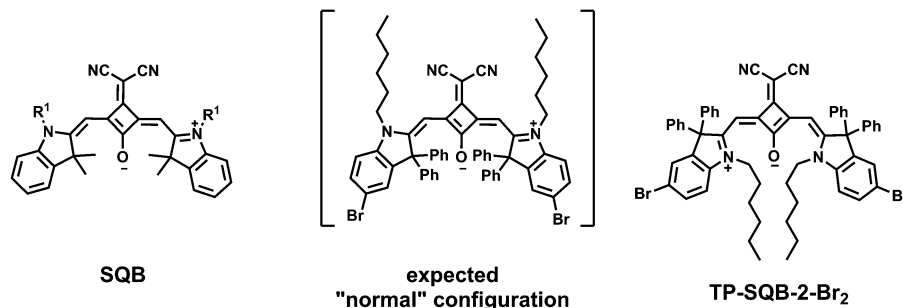
For the monomeric hexyl derivative **TP-SQB-2-Br₂** we were able to grow green crystals from a highly concentrated DCM solution by layering with hexane. Much to our surprise the X-ray crystal structure analysis of these crystals revealed an unusual geometry of the squaraine dye (Fig. 1). While all known *cis*- and *trans*-indolenine squaraines feature a planar geometry with the alkyl-nitrogen groups pointing away from the squaric acid oxygen,^{38–55} in **TP-SQB-2-Br₂** both *N*-alkyl chains point towards the squaric acid core. Moreover, because of steric reasons the indolenine groups are twisted out of the plane thereby avoiding steric congestions of the *N*-alkyl chains with the squaric acid core. This leads to a strongly nonplanar π -system with dihedral angles of the indolenine ring plane and the central squaric acid ring plane of 37.3° and 48.3°, respectively (see Scheme 3). Two of the four phenyl groups point above the squaric acid π -system. The highly twisted π -system also shows some significant deviations of

Scheme 2 Synthesis of squaraines and polysquaraine [TP-SQB]_n.Fig. 1 Molecular structure (top and side view) of TP-SQB-2-Br₂. Hydrogen atoms are omitted for clarity; grey: C, blue: N, red: O, yellow: Br.

the C–C and C–N bond lengths in comparison to “normal” *cis*-squaraines, as can be seen from Table S1 (ESI[†]). Obviously, the reason for this unexpected structure is to avoid steric repulsion of the four phenyl substituents with each other and with the squaric acid oxygen in the expected “normal” squaraine dye configuration (see Scheme 3). Indeed, DFT computations at B3LYP/6-31G* level of theory support these findings (see ESI[†]). The optimized “normal” configuration is also slightly nonplanar (see ESI[†]) because the four phenyl groups try to avoid steric repulsion.

Accordingly, the optimized structure corresponding to the crystal structure is 22.7 kJ mol⁻¹ (0.236 eV) lower in energy than the expected optimized normal configuration reflecting the amount of steric repulsion in the latter. According to the X-ray crystal structure, there are no intermolecular π - π interactions between two different squaraine chromophores highlighting the steric shielding of the squaraine π -system by the four phenyl substituents.

The structure of the polymer was simulated using the semiempirical AM1 Hamiltonian. We optimized two different



Scheme 3 Schematic drawings of different squaraine stereoisomers.

stretched hexamer model structures which differ in the dihedral angle of the biaryl axis between two different squaraine dyes (see Fig. 2). This leads to structure **A** with a large turn of the polymer chain and to structure **B** where the alternating orientation leads to an overall stretched polymer structure. In reality, a mixture of the two structural types within one polymer strand may be present in solution. As we show below, we have evidence that at least two different structural sections exist within one polymer strand which thus is supported by the semiempirical computations. Unlike other polysquaraines, a closely spaced helical structure cannot be formed in the present polymer because the steric repulsion of the four phenyl groups forces the squaraine into the present unusual configuration. The consequence is a much wider angle between two biaryl axes in the polymer which impedes any helix formation with a small number of chromophores per helix turn. From the sketch in Fig. 2 one can estimate that about 10 chromophores would be necessary for one helix turn. However, this is quite unlikely to be formed because disorder will occur before one turn is completed. In comparison in $[\text{SQB}]_n$ one helix turn consists of only about

three chromophores³² which also leads to the formation of cyclic structures.⁵⁶

Steady state optical spectroscopy

The steady state absorption and fluorescence spectra of the **TP-SQB** monomer and polymer in CHCl_3 solution are depicted in Fig. 3 (for data see Table 1). The monomer exhibits typical characteristics of squaraine compounds: an intense main absorption peak at $13\,400\text{ cm}^{-1}$ and a weak shoulder from a vibronic progression on the high energy side with the fluorescence spectra showing a red shift and mirror symmetry. Integration of the absorption band gives a squared transition moment of 85.9 D^2 . The lowest energy absorption band of this squaraine monomer appears to be distinctly redshifted compared to the one of **SQB** which displays an absorption at $14\,600\text{ cm}^{-1}$ with $\epsilon = 1.96 \times 10^5\text{ M}^{-1}\text{ cm}^{-1}$ and $\mu^2 = 98.6\text{ D}^2$. Thus, the distortion of the π -system from planarity leads to a bathochromic shift and a reduced extinction coefficient.⁵⁷

The absorption spectrum of the $[\text{TP-SQB}]_n$ polymer shows a maximum in the near infrared at $12\,400\text{ cm}^{-1}$ with a decent red

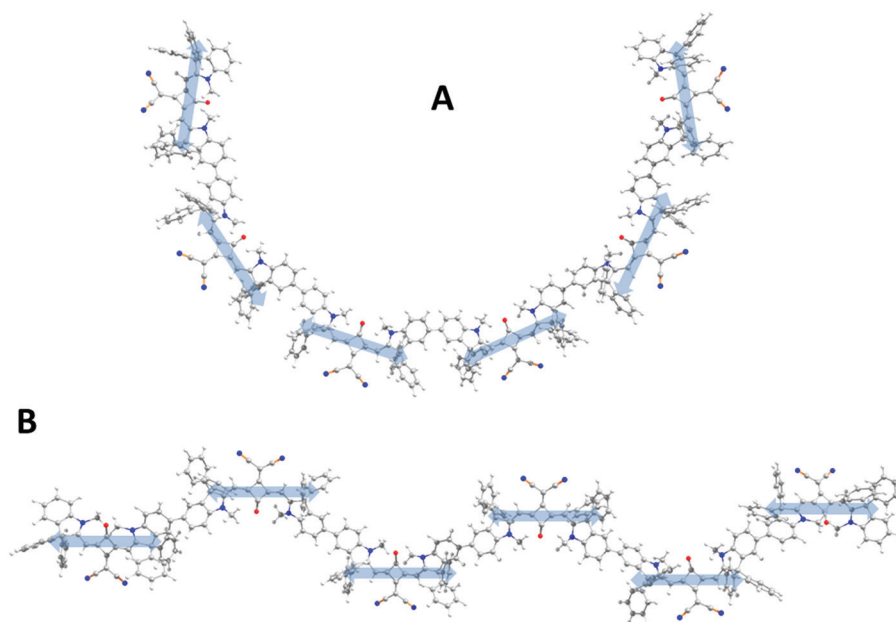


Fig. 2 AM1 computed model hexamers with two different structures caused by the relative dihedral angle between neighboring squaraine dyes. The blue arrows indicate estimated localized transition dipole moments for the localized $S_1 \leftarrow S_0$ transition.

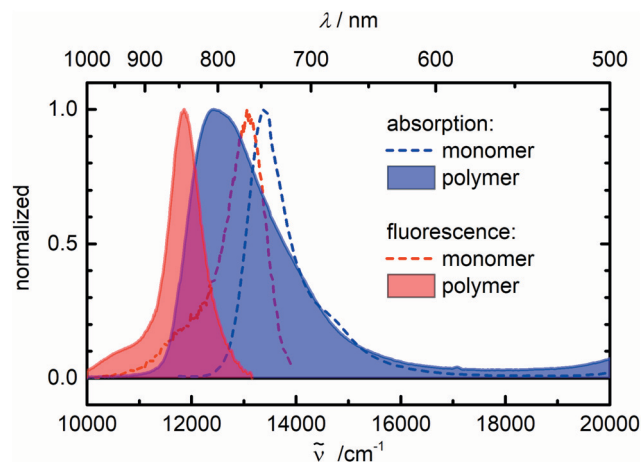


Fig. 3 Absorption and fluorescence spectra of **TP-SQB** monomer and **[TP-SQB]_n** polymer in CHCl_3 .

shift of 1000 cm^{-1} compared to the monomer, which is mainly caused by the exciton splitting of the first excited state. This red shift is similar to the shift observed for covalently linked **SQB** dimers in toluene compared to their monomers (920 cm^{-1} , see Röhr *et al.*⁵⁸) and therefore speaks against a delocalization length beyond that of *ca.* two monomers because an exciton that is delocalized over several monomers would generate a larger splitting of the first excited state according to exciton coupling theory.³⁵ Unlike polymers derived from **SQB**, the absorption oscillator strength of **[TP-SQB]_n** polymer is apparently concentrated in the lower energy edge of the exciton band, while no significant absorption emerges from the upper edge of the exciton band. This hints at a J-type aggregate configuration of the polymers, where the transition moments of the monomers are in a head-to-tail arrangement as expected for a stretched polymer structure. Possible helix structures, as they were observed for **SQB** derived polymers in some solvents, are therefore excluded as they would produce H-type aggregate bands with the largest oscillator strengths at the high energy exciton bands. Such helix foldamers with a small pitch are disfavoured because of steric repulsion of the phenyl groups extending almost perpendicularly from the π -plane (see Fig. 1) which induces the present distorted squaraine conformation leading to a much wider biaryl–biaryl angle in the polymer. Integration of the lowest energy absorption band and taking the degree of polymerization into account yields the squared transition dipole moment⁵⁹ $\mu^2 = 89.3 \text{ D}^2$ per monomer in very good agreement with the monomer. Unlike **[SQB]_n** polymer, the solvatochromic response of **TP-SQB** and **[TP-SQB]_n** is rather weak, that is, the

absorption band shape of the monomer is hardly affected by the solvent and the maximum varies only between $13\,100 \text{ cm}^{-1}$ (toluene) and $13\,500 \text{ cm}^{-1}$ (DMF). Quite similar observations were made for the polymer in a series of solvents (toluene, *o*DCB, PhCN, CHCl_3 , DCM, acetone, DMF, see ESI†). These little changes are attributed to stabilization of the excited state by more polarizable solvents.

A closer look at the absorption band of the polymer reveals a double peak structure at *ca.* $12\,500 \text{ cm}^{-1}$, which is visible as two merging peaks forming a plateau at the peak maximum, which has to be discussed in further detail below. A possible explanation would be the existence of two different, though energetically very similar, monomer–monomer conformers within the polymer strands. These conformers may be formed by a rotation around the central biaryl axis connecting the individual squaraine dyes as anticipated by the AM1 calculations, see above. Indeed, CNDO S2 calculations based on these structural models predict J-type exciton bands for both conformers but the absorption maximum of the exciton manifold is 500 cm^{-1} lower energy for structure **B** than for structure **A** (see ESI†).

The fluorescence spectrum of the **[TP-SQB]_n** polymer roughly resembles the shape of the monomer fluorescence and seems to originate exclusively from the lowest lying exciton states, showing a Stokes shift of 560 cm^{-1} . This is more than the monomer Stokes shift of 340 cm^{-1} and is therefore in contradiction with results from other J-aggregates, where the delocalization of the exciton leads to smaller Stokes shift compared to the respective monomers. The full width at half maximum (fwhm) of the polymer fluorescence band (720 cm^{-1}) is smaller than that of the monomer (860 cm^{-1}). According to the $N^{-1/2}$ relation,^{60–63} this indicates a delocalization length of only ~ 1.4 monomers and, thus also points against a long delocalization length. On the other hand, this criterion is not very reliable because of the inhomogeneity (polydispersity) of the polymer sample.

Both monomer and polymer display a rather small fluorescence quantum yield of 0.02 and 0.04, respectively, which is distinctly smaller than that of *e.g.* **SQB** with 0.55. Using the lifetime and the quantum yield we also calculated the squared fluorescence transition dipole moment⁵⁹ (see Table 1) which is smaller for the monomer but larger for the polymer. The former may hint towards structural distortion in the monomer excited state which reduces the effective overlap of excited and ground state wave function and the latter confirms the delocalization of the exciton over a few monomers because the transition dipole moment should ideally be additive with the number of chromophores involved in the excited state. In fact, the ratio of $\mu_{\text{fl}}^2/\mu_{\text{abs}}^2 \sim 3.7$ is larger than the delocalization length estimated above from the exchange

Table 1 Absorption ($\tilde{\nu}_{\text{abs}}$) and fluorescence ($\tilde{\nu}_{\text{fl}}$) maxima, fluorescence lifetimes (τ_{fl}) amplitude (*a*) and quantum yield (Φ_{fl}) of **TP-SQB** monomers and **[TP-SQB]_n** polymer in CHCl_3

	$\tilde{\nu}_{\text{abs1}}/\text{cm}^{-1}$ [$\epsilon/\text{M}^{-1} \text{ cm}^{-1}$]	$\tilde{\nu}_{\text{abs2}}/\text{cm}^{-1}$	$\mu_{\text{abs}}^2/\text{D}^2$	$\tilde{\nu}_{\text{fl}}/\text{cm}^{-1}$	$\tau_{\text{fl}}^a/\text{ns}$ (<i>a</i>)	$\tau_{\text{fl2}}^a/\text{ns}$ (<i>a</i>)	Φ_{fl}	$\mu_{\text{fl}}^2/\text{D}^2$
TP-SQB	13 400 [1.37×10^5]	13 700	85.9	13 100	0.20 (0.97)	1.81 (0.03)	0.02 ± 0.014	57.8
[TP-SQB]_n	12 400 [7.66×10^4]	12 700	89.3	11 900	0.12 (0.94)	0.33 (0.06)	0.04 ± 0.014	216.5

^a Measured by TCSPC.

narrowing. However, we have to stress that the accuracy is limited in this case because the low fluorescence quantum yield is afflicted with a major error (see Table 1).

Time resolved optical spectroscopy

The fluorescence lifetimes of both monomer and polymer were measured in CHCl_3 solution using time correlated single photon counting method (TCSPC) with excitation at $15\,200\text{ cm}^{-1}$ (IRF = 0.27 ns). The monomer shows a predominant lifetime of $\tau = 0.20\text{ ns}$

and a very small component of 1.8 ns . This contrasts the lifetime of “normal” SQB with $\tau = 2.40\text{ ns}$ and explains the rather small fluorescence quantum yield of the former. The polymer also has an even shorter lifetime of 0.12 ns as the principal component.

In order to get a closer look into the photoinduced dynamics at shorter times we performed transient absorption spectroscopy with fs-time resolution in CHCl_3 . The transient absorption measurements of the monomer (see Fig. 4) are dominated by a strong negative feature peaking at around $13\,200\text{ cm}^{-1}$,

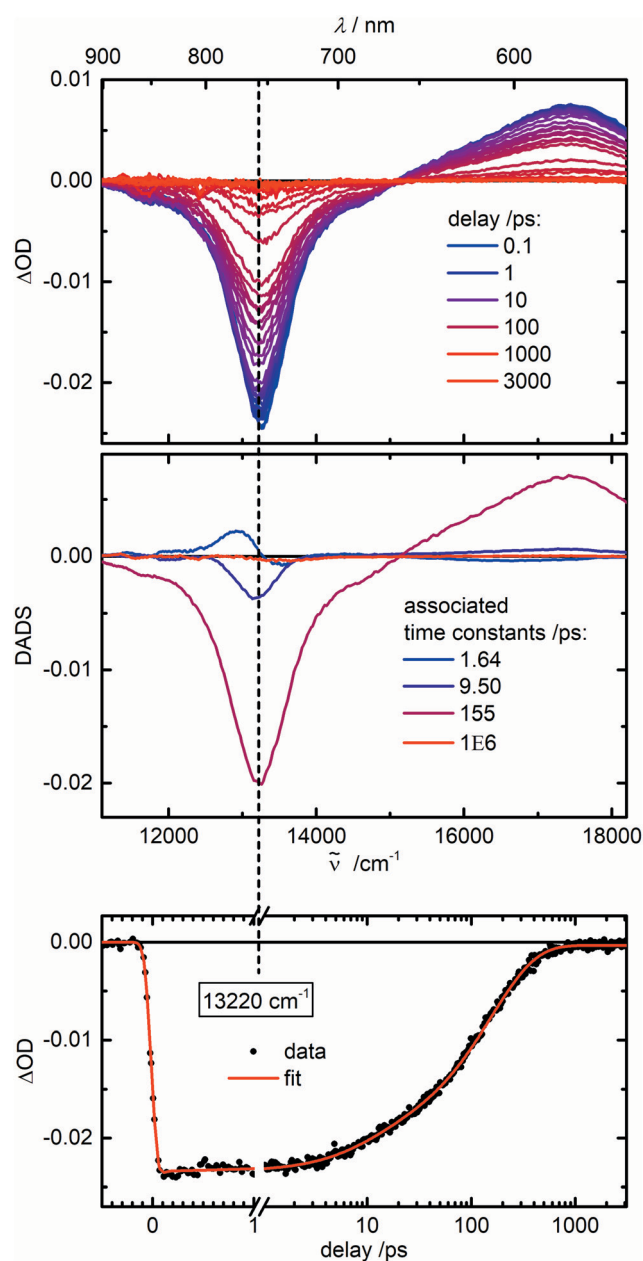


Fig. 4 Top panel: Transient absorption spectra of TP-SQB monomer in CHCl_3 after excitation at $13\,400\text{ cm}^{-1}$, probed under magic angle. Middle panel: Decay associated difference spectra (DADS) from a global fit of the transient absorption spectra of TP-SQB monomer in CHCl_3 with associated time constants τ . Lower panel: Transient absorption time trace at $13\,200\text{ cm}^{-1}$ and corresponding fit curve from the global fit.

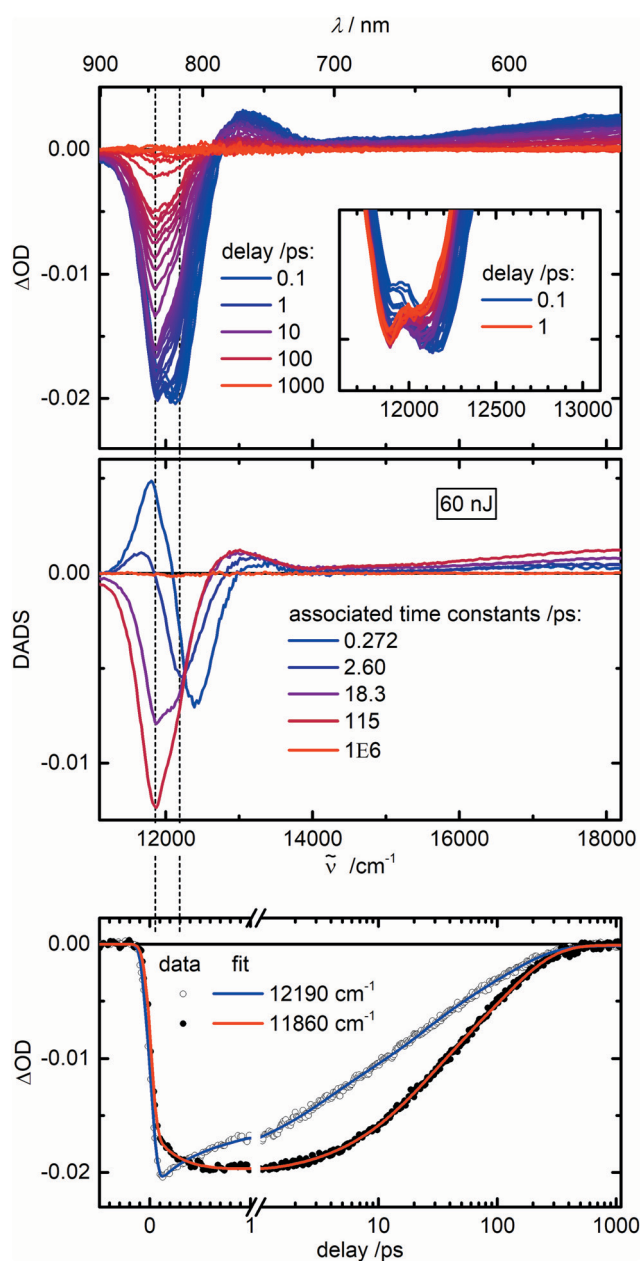


Fig. 5 Top panel: Transient absorption spectra of $[\text{TP-SQB}]_n$ polymer in CHCl_3 after excitation at $12\,500\text{ cm}^{-1}$ with a pump pulse energy of 60 nJ , probed under magic angle. Middle panel: DADS from a global fit of the transient absorption spectra of $[\text{TP-SQB}]_n$ polymer in CHCl_3 with associated time constants τ . Lower panel: Transient absorption time traces at selected wavenumbers and corresponding fit curves from the global fit.

between the absorption and the fluorescence maximum (13 400 and 13 100 cm^{-1} , respectively, see Table 1). This is the sum of ground state bleaching (GSB) and stimulated emission (SE). At higher wavenumbers, excited state absorption (ESA) can be observed with a maximum at around 17 400 cm^{-1} .

A global exponential fit of the transient data of the monomer yields decay associated difference spectra (DADS)⁶⁴ revealing small spectral shifts in the first picoseconds, parametrized with two time constants of 1.64 and 9.5 ps, and a monoexponential decay to the ground state with a time constants of 155 ps. The latter is the dominant decay time and agrees nicely with the fluorescence lifetime of 200 ps (see Table 1). A time constant with 1×10^6 ps, which serves as an offset on the timescale of the measurement, was added to compensate for improper scatter correction. This component shows a very small amplitude in the spectral region of the excitation pulse.

The transient absorption spectra of the polymer show a strong negative signal around 12 000 cm^{-1} , stemming from GSB and SE (see Fig. 5). At higher wavenumbers, the spectra are dominated by ESA. The small peak at 13 200 cm^{-1} is caused by a two-photon state as observed before in such polymers.³¹ At short times, the negative signal around 12 000 cm^{-1} exhibits a double peak structure with an energy difference (12 200–11 900 $\text{cm}^{-1} = 300 \text{ cm}^{-1}$) which is in reasonable agreement with the one calculated with the CINDO S2 method (see above). Here the peak on the red side rises concurrently with the decay of the peak on the blue side. Thereby, an isosbestic point seems to appear between the peaks at 12 000 cm^{-1} (see inset, Fig. 5). This is an indication for energy transfer between two species (or two states) rather than for vibrational or geometric relaxation processes in the excited state, which are the common cause for a Stokes shift. A continuous shift of the red side of the joint GSB

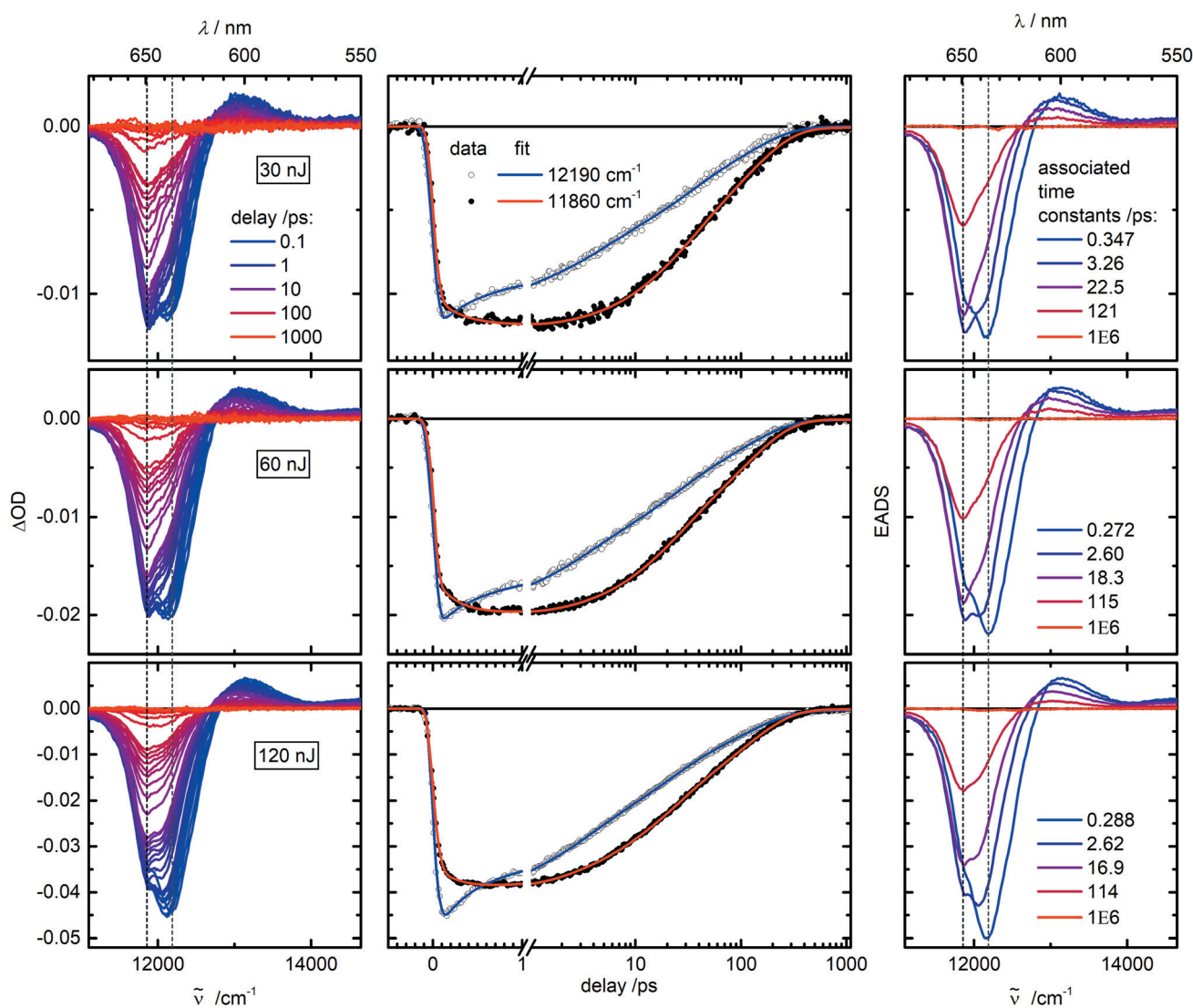


Fig. 6 Left column: Transient absorption spectra of [TP-SQB]_n polymer in CHCl₃ after excitation at 12 500 cm^{-1} with a pump pulse energies of 30, 60 and 120 nJ, probed under magic angle. Middle panel: Transient absorption time traces at selected wavenumbers and corresponding fit curves from the global fit. Right column: EADS from the global fits of the transient absorption spectra with associated time constants τ .

and SE signal along with a broadening would be expected instead of the occurrence of a second peak. The second peak, on the other hand, could support the notion of different monomer–monomer configurations which also serves to explain the double peak in the steady state absorption spectra. That might also be the reason for the relatively large Stokes shift. Hence, a section within the polymer strand is postulated which possesses a specific configuration with an excited state being lower in energy than the surrounding polymer sections and which therefore acts as an excitation trap. A prerequisite for this exciton trapping effect would be that the excitations within the polymer strands are mobile.

A global exponential fit of the transient data shows four time constants (a fifth one of 1×10^6 ps is used to account for improper scatter correction) in the range from ~ 0.3 ps up to ~ 120 ps whereby the latter is in good agreement with the fluorescence lifetime (see Table 1). Fig. 5 (middle panel) presents the DADS of the time constants. The DADS show, that especially the shortest time constant of ~ 0.3 ps is associated with the above described decay of signal strength at the blue side of the main transient absorption band and the concurring rise of (negative) signal strength on the red side, which indicates a transition from a higher to a lower excited state along with excitation energy transfer between different sites of the polymer. However, the second DADS associated with a time constant of 2.6 ps also shows these characteristics to some extent. Therefore, the DADS illustrate energy transfer dynamics, which are obviously not single exponential. This hints at a diffusion controlled process like exciton trapping, too. This kind of energy transfer is on a similar time scale as exciton localization processes which are believed to take place on the order of 100 fs. On the other hand, intrachain energy transfer should be on the order of tens ps to hundreds of ps.⁶⁵

Transient absorption measurements with different pump pulse energies of 30, 60 and 120 nJ, *i.e.* different pump intensities (see Fig. 6), reveal a change in the relative signal strength within the double peak structure: with increasing pump intensity, the relative strength of the low energy peak decreases compared to the strength of the high energy peak (see also Fig. 7). A possible explanation could be a saturation of the state or species associated with the low energy peak. Another effect, that can be observed, is a slight excitation intensity dependence of the dynamics, which appear to be faster at higher intensities (see Fig. 7). This is typical of exciton–exciton annihilation speaking again for mobile excitons.^{31,66–73} However, the saturation effect alone might be responsible for the different dynamics. On the other hand, fast exciton–exciton–annihilation could act as a decay channel for the energetically higher lying state, competing with relaxation to the lower state and thus increasingly suppressing SE from the latter with increasing excitation intensity.

The time constants from a global fit of the three data sets shorten slightly with rising excitation intensity, reflecting the intensity dependence of the dynamics (see Fig. 7). Moreover, the relative amplitudes of the evolution associated difference spectra (EADS)⁷⁴ change, probably partly due to the change in dynamics as well as due to the saturation effect that is observable

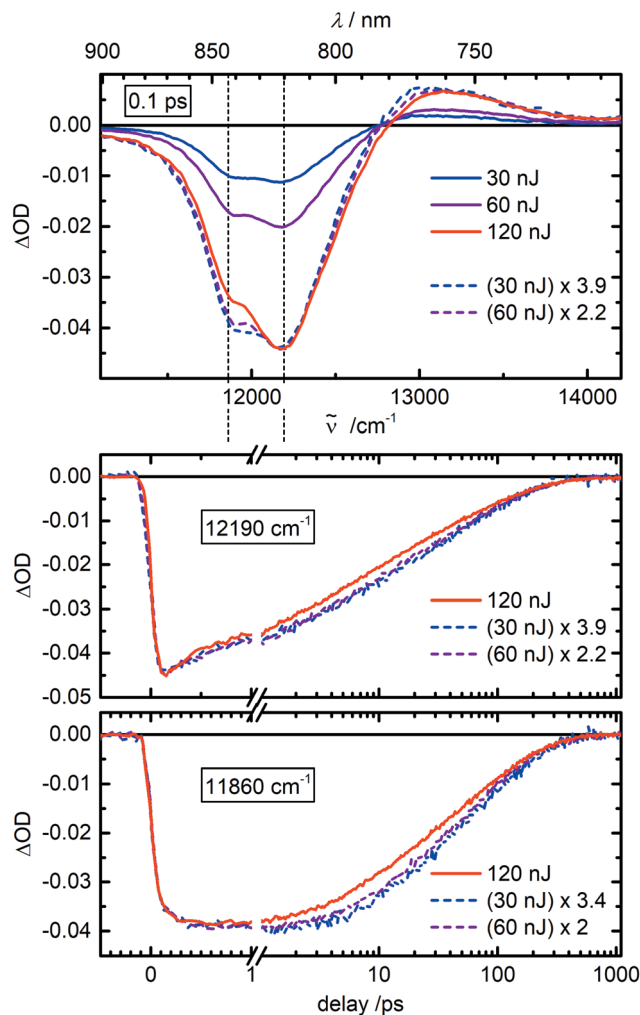


Fig. 7 Comparison of transient absorption spectra at 0.1 ps (top) and selected time traces of [TP-SQB]_n polymer in CHCl₃ after excitation at 12 500 cm⁻¹ with different excitation pulse energies (30, 60, and 120 nJ). The traces are scaled according to the factors given in the legend.

at the low energy peak (see Fig. 7, upper panel). While a detailed analysis of the possible exciton annihilation process is beyond the scope of this work we state here that we are confident that our interpretation of the energy transfer processes between the two different polymer sections is not afflicted neither quantitatively nor quantitatively by the annihilation.

Conclusion

A squaraine polymer was synthesized which, owing to the structure of the monomer, may contain stretched or slightly bent sections. Within one polymer strand these sections possess slightly different excited state energies. This leads to a broad absorption band for the exciton manifold where two peaks can be identified which may be associated with the two conformational structures. Excitation of the higher energy band populated the excited state of the one section and is followed by a biphasic energy transfer (0.3 and 2.6 ps) to the section with the lower

energy band. Variation of the pump intensity shows saturation of the section with the lower energy excited state supporting the energy transfer model between different sections rather than an internal conversion process within one section. The exciton annihilation responsible for the intensity dependent decay times also proves the high mobility of the excitons. The energy transfer rates are on the same order of magnitude as observed in other conjugated polymers^{75–79} such as MEH-PPV but are slower than in a squaraine copolymer [SQA-SQB]_n composed of *trans*- and *cis*-indolenine squaraine dyes for which we estimated exciton transfer rates of about (30 fs)⁻¹.³¹ The latter also shows significant exchange narrowing of the absorption band which is most likely caused by a high structural order but is almost absent in the present polymer owing to a much smaller delocalization length which may also be responsible for the much slower energy transfer rate. However, for the [SQB]_n homopolymer we found, depending on the solvent and the specific pathway, energy transfer rates between (70 fs)⁻¹ and (4 ps)⁻¹.³² Thus, in terms of energy transfer rates, the [TP-SQB]_n polymer behaves more like the [SQB]_n homopolymer and other more conventional highly disordered conjugated polymers.

Conflicts of interest

There are no conflicts to declare.

Acknowledgements

We acknowledge funding by the Deutsche Forschungsgemeinschaft within the Research Group FOR 1809 and the Bavarian State Ministry of Science, Research and the Arts within the SolTech network.

References

- L. Ying, F. Huang and G. C. Bazan, *Nat. Commun.*, 2017, **8**, 14047.
- L. Dou, Y. Liu, Z. Hong, G. Li and Y. Yang, *Chem. Rev.*, 2015, **115**, 12633–12665.
- X. Guo, M. Baumgarten and K. Müllen, *Prog. Polym. Sci.*, 2013, **38**, 1832–1908.
- O. Ostroverkhova, *Chem. Rev.*, 2016, **116**, 13279–13412.
- M. Y. Wong, *J. Electron. Mater.*, 2017, **46**, 6246–6281.
- R. Hildner, A. Köhler, P. Müller-Buschbaum, F. Panzer and M. Thelakkat, *Adv. Energy Mater.*, 2017, **7**, 1700314.
- Y.-J. Cheng, S.-H. Yang and C.-S. Hsu, *Chem. Rev.*, 2009, **109**, 5868–5923.
- P.-L. T. Boudreault, A. Najari and M. Leclerc, *Chem. Mater.*, 2011, **23**, 456–469.
- S. Inal, J. Rivnay, A.-O. Suiu, G. G. Malliaras and I. McCulloch, *Acc. Chem. Res.*, 2018, **51**, 1368–1376.
- M. Li, C. An, W. Pisula, K. Müllen and W. Pisula, *Acc. Chem. Res.*, 2018, **51**, 1196–1205.
- Y. Xu, H. Sun, W. Li, Y.-F. Lin, F. Balestra, G. Ghibaud and Y.-Y. Noh, *Adv. Mater.*, 2017, **29**, 1702729.
- B. Walker, C. Kim and T.-Q. Nguyen, *Chem. Mater.*, 2011, **23**, 470–482.
- S. F. Völker, S. Uemura, M. Limpinsel, M. Mingeback, C. Deibel, V. Dyakonov and C. Lambert, *Macromol. Chem. Phys.*, 2010, **211**, 1098–1108.
- U. Mayerhöffer, K. Deing, K. Gruss, H. Braunschweig, K. Meerholz and F. Würthner, *Angew. Chem., Int. Ed.*, 2009, **48**, 8776–8779.
- T. Maeda, T. Tsukamoto, A. Seto, S. Yagi and H. Nakazumi, *Macromol. Chem. Phys.*, 2012, **213**, 2590–2597.
- T. Maeda, Y. Hamamura, K. Miyanaga, N. Shima, S. Yagi and H. Nakazumi, *Org. Lett.*, 2011, **13**, 5994–5997.
- T. Maeda, T. V. Nguyen, Y. Kuwano, X. Chen, K. Miyanaga, H. Nakazumi, S. Yagi, S. Soman and A. Ajayaghosh, *J. Phys. Chem. C*, 2018, **122**, 21745–21754.
- G. Wei, S. Wang, K. Sun, M. E. Thompson and S. R. Forrest, *Adv. Energy Mater.*, 2011, **1**, 184–187.
- M. Gsänger, D. Bialas, L. Huang, M. Stolte and F. Würthner, *Adv. Mater.*, 2016, **28**, 3615–3645.
- G. Chen, C. Si, P. Zhang, B. Wei, J. Zhang, Z. Hong, H. Sasabe and J. Kido, *Org. Electron.*, 2017, **51**, 62–69.
- G. Chen, H. Sasabe, T. Igarashi, Z. Hong and J. Kido, *J. Mater. Chem. A*, 2015, **3**, 14517–14534.
- G. Chen, H. Sasabe, W. Lu, X.-F. Wang, J. Kido, Z. Hong and Y. Yang, *J. Mater. Chem. C*, 2013, **1**, 6547–6552.
- M. Gsänger, E. Kirchner, M. Stolte, C. Burschka, V. Stepanenko, J. Pflaum and F. Würthner, *J. Am. Chem. Soc.*, 2014, **136**, 2351–2362.
- S. Sreejith, P. Carol, P. Chithra and A. Ajayaghosh, *J. Mater. Chem.*, 2008, **18**, 264–274.
- L. Beverina and P. Salice, *Eur. J. Org. Chem.*, 2010, 1207–1225.
- W. Li, K. H. Hendriks, M. M. Wienk and R. A. J. Janssen, *Acc. Chem. Res.*, 2016, **49**, 78–85.
- M. H. Schreck, M. I. S. Röhr, T. Clark, V. Stepanenko, F. Würthner and C. Lambert, *Chem. – Eur. J.*, 2019, **25**, 2831–2839.
- T. Brixner, R. Hildner, J. Köhler, C. Lambert and F. Würthner, *Adv. Energy Mater.*, 2017, **7**, 1700236.
- L. J. Patalag, L. P. Ho, P. G. Jones and D. B. Werz, *J. Am. Chem. Soc.*, 2017, **139**, 15104–15113.
- N. Sakamoto, C. Ikeda, M. Yamamura and T. Nabeshima, *Chem. Commun.*, 2012, **48**, 4818–4820.
- S. F. Völker, A. Schmiedel, M. Holzapfel, K. Renziehausen, V. Engel and C. Lambert, *J. Phys. Chem. C*, 2014, **118**, 17467–17482.
- C. Lambert, F. Koch, S. F. Völker, A. Schmiedel, M. Holzapfel, A. Humeniuk, M. I. S. Röhr, R. Mitric and T. Brixner, *J. Am. Chem. Soc.*, 2015, **137**, 7851–7861.
- D. J. Harkin, K. Broch, M. Schreck, H. Ceymann, A. Stoy, C. K. Yong, M. Nikolka, I. McCulloch, N. Stingelin, C. Lambert and H. Sirringhaus, *Adv. Mater.*, 2016, **28**, 6378–6385.
- Foldamers*, ed. S. Hecht and I. Huc, Wiley-VCH Verlag GmbH & Co. KGaA, Weinheim, 2007.
- M. Kasha, H. R. Rawls and M. Ashraf El-Bayoumi, *Pure Appl. Chem.*, 1965, **11**, 371.
- T.-S. Ahn, R. O. Al-Kaysi, A. M. Muller, K. M. Wentz and C. J. Bardeen, *Rev. Sci. Instrum.*, 2007, **78**, 086105.

- 37 T. Maeda, S. Nitta, Y. Sano, S. Tanaka, S. Yagi and H. Nakazumi, *Dyes Pigm.*, 2015, **122**, 160–167.
- 38 U. Mayerhöffer, K. Deing, K. Gruss, H. Braunschweig, K. Meerholz and F. Würthner, *Angew. Chem., Int. Ed.*, 2009, **48**, 8776–8779.
- 39 U. Mayerhöffer, M. Gsänger, M. Stolte, B. Fimmel and F. Würthner, *Chem. – Eur. J.*, 2013, **19**, 218–232.
- 40 U. Mayerhöffer, B. Fimmel and F. Würthner, *Angew. Chem., Int. Ed.*, 2012, **51**, 164–167.
- 41 T. Maeda, S. Mineta, H. Fujiwara, H. Nakao, S. Yagi and H. Nakazumi, *J. Mater. Chem. A*, 2013, **1**, 1303–1309.
- 42 D. E. Lynch and K. A. Byriel, *Cryst. Eng.*, 2000, **2**, 225–239.
- 43 D. E. Lynch, *Acta Crystallogr., Sect. E: Struct. Rep. Online*, 2002, **58**, o1025–o1027.
- 44 M. Matsui, M. Fukushima, Y. Kubota, K. Funabiki and M. Shiro, *Tetrahedron*, 2012, **68**, 1931–1935.
- 45 D. E. Lynch, A. N. Kirkham, J. Heptinstall and M. J. Cox, *Dyes Pigm.*, 2013, **99**, 160–167.
- 46 D. E. Lynch, M. J. Cox, P. M. King and G. Smith, *J. Photochem. Photobiol., A*, 2016, **324**, 87–95.
- 47 D. E. Lynch, M. Cox and P. M. King, *J. Photochem. Photobiol., A*, 2018, **360**, 224–230.
- 48 D. E. Lynch, A. N. Kirkham, M. Z. H. Chowdhury, E. S. Wane and J. Heptinstall, *Dyes Pigm.*, 2012, **94**, 393–402.
- 49 O. S. Kolosova, S. V. Shishkina, V. Marks, G. Gellerman, I. V. Hovor, A. L. Tatarets, E. A. Terpetschnig and L. D. Patsenker, *Dyes Pigm.*, 2019, **163**, 318–329.
- 50 G. Smith and D. E. Lynch, *Acta Crystallogr., Sect. E: Struct. Rep. Online*, 2013, **69**, o786–o787.
- 51 A. Punzi, M. A. M. Capozzi, V. Fino, C. Carlucci, M. Suriano, E. Mesto, E. Schingaro, E. Orgiu, S. Bonacchi, T. Leydecker, P. Samori, R. Musio and G. M. Farinola, *J. Mater. Chem. C*, 2016, **4**, 3138–3142.
- 52 K. Ueji, S. Ichimura, Y. Tamaki and K. Miyamura, *CrystEngComm*, 2014, **16**, 10139–10147.
- 53 U. Lawrentz, W. Grahn, I. Dix and P. G. Jones, *Acta Crystallogr., Sect. C: Cryst. Struct. Commun.*, 2001, **C57**, 126–128.
- 54 Y. Xu, M. J. Panzner, X. Li, W. J. Youngs and Y. Pang, *Chem. Commun.*, 2010, **46**, 4073–4075.
- 55 P. F. Santos, L. V. Reis, P. Almeida and D. E. Lynch, *CrystEngComm*, 2011, **13**, 1333–1338.
- 56 C. Brüning, E. Welz, A. Heilos, V. Stehr, C. Walter, B. Engels, S. F. Völker, C. Lambert and V. Engel, *J. Phys. Chem. C*, 2015, **119**, 6174–6180.
- 57 J. Fabian and R. Zahradník, *Angew. Chem., Int. Ed. Engl.*, 1989, **28**, 677–694.
- 58 M. I. S. Röhr, H. Marciniak, J. Hoche, M. H. Schreck, H. Ceymann, R. Mitric and C. Lambert, *J. Phys. Chem. C*, 2018, **122**, 8082–8093.
- 59 H. Marciniak, N. Auerhammer, S. Ricker, A. Schmiedel, M. Holzapfel and C. Lambert, *J. Phys. Chem. C*, 2019, **123**, 3426–3432.
- 60 This relation only allows a rough estimate of the coherence length. See: E. W. Knapp, *Chem. Phys.*, 1984, **85**, 73–82; P. B. Walczak, A. Eisfeld and J. S. J. Briggs, *Chem. Phys.*, 2008, **128**, 044505; G. D. Scholes and C. J. Smyth, *Chem. Phys.*, 2014, **140**, 11901.
- 61 J. A. Leegwater, *J. Phys. Chem.*, 1996, **100**, 14403–14409.
- 62 E. Rousseau, M. Van der Auweraer and F. C. De Schryver, *Langmuir*, 2000, **16**, 8865–8870.
- 63 J. Knoester, *Proc. Int. Sch. Phys. “Enrico Fermi”*, 2002, **149**, 149–186.
- 64 Decay associated difference spectra refer to a kinetic model in which all species decay in parallel. The amplitudes of the multiexponential decay constitute the DADS.
- 65 I. Hwang and G. D. Scholes, *Chem. Mater.*, 2011, **23**, 610–620.
- 66 K. Hader, V. May, C. Lambert and V. Engel, *Phys. Chem. Chem. Phys.*, 2016, **18**, 13368–13374.
- 67 Y. Zaushtsyn, K. G. Jespersen, L. Valkunas, V. Sundstrom and A. Yartsev, *Phys. Rev. B: Condens. Matter Mater. Phys.*, 2007, **75**, 195201.
- 68 D. C. Dai and A. P. Monkman, *Phys. Rev. B: Condens. Matter Mater. Phys.*, 2013, **87**, 045308.
- 69 M. A. Stevens, C. Silva, D. M. Russell and R. H. Friend, *Phys. Rev. B: Condens. Matter Mater. Phys.*, 2001, **63**, 165213.
- 70 S. Cook, H. Liyuan, A. Furube and R. Katoh, *J. Phys. Chem. C*, 2010, **114**, 10962–10968.
- 71 A. J. Lewis, A. Ruseckas, O. P. M. Gaudin, G. R. Webster, P. L. Burn and I. D. W. Samuel, *Org. Electron.*, 2006, **7**, 452–456.
- 72 D. Peckus, A. Devizis, D. Hertel, K. Meerholz and V. Gulbinas, *Chem. Phys.*, 2012, **404**, 42–47.
- 73 S. Gelinis, J. Kirkpatrick, I. A. Howard, K. Johnson, M. W. B. Wilson, G. Pace, R. H. Friend and C. Silva, *J. Phys. Chem. B*, 2013, **117**, 4649–4653.
- 74 Evolution associated difference spectra refer to a kinetic model in which all species evolve sequentially in time with increasing time constants. The amplitudes of the multiexponential model constitute the EADS.
- 75 E. Hennebicq, G. Pourtois, G. D. Scholes, L. M. Herz, D. M. Russell, C. Silva, S. Setayesh, A. C. Grimsdale, K. Muellen, J.-L. Bredas and D. Beljonne, *J. Am. Chem. Soc.*, 2005, **127**, 4744–4762.
- 76 D. Beljonne, G. Pourtois, C. Silva, E. Hennebicq, L. M. Herz, R. H. Friend, G. D. Scholes, S. Setayesh, K. Müllen and J. L. Bredas, *Proc. Natl. Acad. Sci. U. S. A.*, 2002, **99**, 10982–10987.
- 77 K. Becker and J. M. Lupton, *J. Am. Chem. Soc.*, 2006, **128**, 6468–6479.
- 78 M. M. L. Grage, P. W. Wood, A. Ruseckas, T. Pullerits, W. Mitchell, P. L. Burn, I. D. W. Samuel and V. Sundstrom, *J. Chem. Phys.*, 2003, **118**, 7644–7650.
- 79 J. R. Miller, A. R. Cook, K. S. Schanze and P. Sreearunothai, in *Charge and Exciton Transport through Molecular Wires*, ed. L. D. A. Siebbeles and F. C. Grozema, John Wiley & Sons, Inc., 2011.